

## A wirelessly readable and resettable shock recorder through the integration of LC circuits and MEMS devices

This content has been downloaded from IOPscience. Please scroll down to see the full text.

2014 *Smart Mater. Struct.* 23 095030

(<http://iopscience.iop.org/0964-1726/23/9/095030>)

[View the table of contents for this issue](#), or go to the [journal homepage](#) for more

Download details:

IP Address: 140.113.38.11

This content was downloaded on 25/12/2014 at 01:32

Please note that [terms and conditions apply](#).

# A wirelessly readable and resettable shock recorder through the integration of LC circuits and MEMS devices

**Sung-Yueh Wu, Chen-Yuan Hung and Wensyang Hsu**

Department of Mechanical Engineering, National Chiao Tung University, 1001 Ta Hsueh Road, Hsinchu 300, Taiwan

E-mail: [whsu@mail.nctu.edu.tw](mailto:whsu@mail.nctu.edu.tw)

Received 19 May 2014, revised 18 June 2014

Accepted for publication 8 July 2014

Published 14 August 2014

## Abstract

This paper presents a passive shock recorder to record shock events for tens of Gs with wireless reading and wireless resetting capabilities through the integration of LC circuits and two MEMS devices. With a micro mechanical-latch shock switch electrically connected to the sensing LC circuit, the shock event that leads to different latching states can be recorded and wirelessly read through the LC resonant frequency. With a micro electro-thermal actuator electrically connected to a wirelessly powered actuating LC circuit, the energy can be wirelessly sent to the micro actuator to provide the necessary unlatched force. By integrating the mechanical-latch shock switch and actuator with LC circuits, the latching state can be reset through the wireless actuation. Therefore, the shock recorder can be used repeatedly. Here, the mechanical-latch shock switch is designed to have a two-level shock recording capability. The fabrication of the shock switch and actuator are achieved by a Ni-based surface micromachining process. When the acceleration reaches 28.06 G, the latching state changes from the original state to the first latching state. The resonant frequency of sensing for the LC circuit is found to switch from 10.14 MHz to 9.16 MHz, correspondingly. By further applying acceleration up to 37.10 G, the latching state changes from the first latching state to the second state, and the resonant frequency shifts to 7.83 MHz. Then, with a current of 2.07 A<sub>AC</sub> wirelessly induced in the actuating LC circuit, the micro electro-thermal actuator is shown to provide sufficient displacement to reset the shock switch from a latched state back to the original unlatched state, and the resonant frequency is switched back to 10.14 MHz. The fabricated shock recorder is repeatedly tested five times. The wireless reading, resetting and shock recording capabilities are successfully verified.

Keywords: LC transducers, shock switch, electro-thermal actuator

## 1. Introduction

Inductor-capacitor (LC) transducers have attracted a lot of attention due to their wireless and passive capabilities. Without a battery or other power supply electrically connected to the devices, LC transducers, which are different from active wireless transducers that need an on-board power supply [1–3], are more suitable for placing at sealing chambers to avoid battery replacement or maintenance.

LC sensors have been developed for the sensing of various environmental variations, such as pressure [4–11], strain [12–16], humidity [4, 6, 17–19], temperature [4, 17, 20],

pH [21, 22], bacteria [23] or specific gases [24]. The operating process of typical LC sensors is shown in figure 1(a). With a network analyzer applying an oscillating signal to the transmitter, the oscillating magnetic flux can be generated in nearby space. By inductively coupling the transmitter and the inductor of the receiving LC circuit, forward electromotive forces are induced wirelessly in the receiving inductor, based on Faraday's law. Therefore, the LC circuit can receive energy through the inductor and store it in the capacitor. With this energy, the magnetic flux can also be generated by the LC circuit itself; then, the backward electromotive forces can be induced on the transmitter wirelessly, affecting the charge

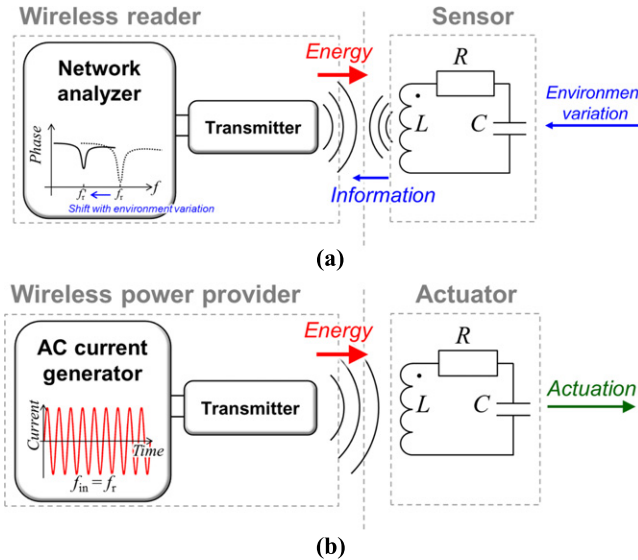


**Figure 1.** Schematic illustrations of LC transducers: (a) LC sensor; (b) LC actuator.

flow in the transmitter. Since both the forward and backward electromotive forces reach a maximum at resonant frequency  $f$  of the LC circuit, listed as equation (1) [4], the frequency response of the transmitter changes abruptly at  $f$ ; therefore,

the resonant frequency can be determined.

$$f = \frac{1}{2\pi\sqrt{LC}} \quad (1)$$

When the inductance  $L$  or the capacitance  $C$  of the LC circuit is affected by physical or chemical conditions, the resonant frequency  $f$  of the LC circuit will be changed. Then, the LC circuit can act as an LC sensor. Since the LC circuit can receive energy wirelessly, especially at resonant frequency  $f$ , the LC circuit can also work as an actuator by further utilizing the received energy, as shown in figure 1(b). With the received energy, high voltage or Joule heating are commonly transduced for different kinds of actuations, such as wirelessly powered micro robots [25, 26] and implantable drug delivery devices [27–29].

Recently, Kuo *et al* proposed an inertial switch with wireless readability [30], which can be applied for recording if the acceleration of a parcel exceeds a specified acceleration threshold during transportation. With this wireless readability, the recorded information can be obtained wirelessly, which is relatively efficient when there are many parcels to be read. However, if the wireless shock switch needs to be placed in a sealed environment where the switch is hard to replace, such as an embedded concrete structure for structure health

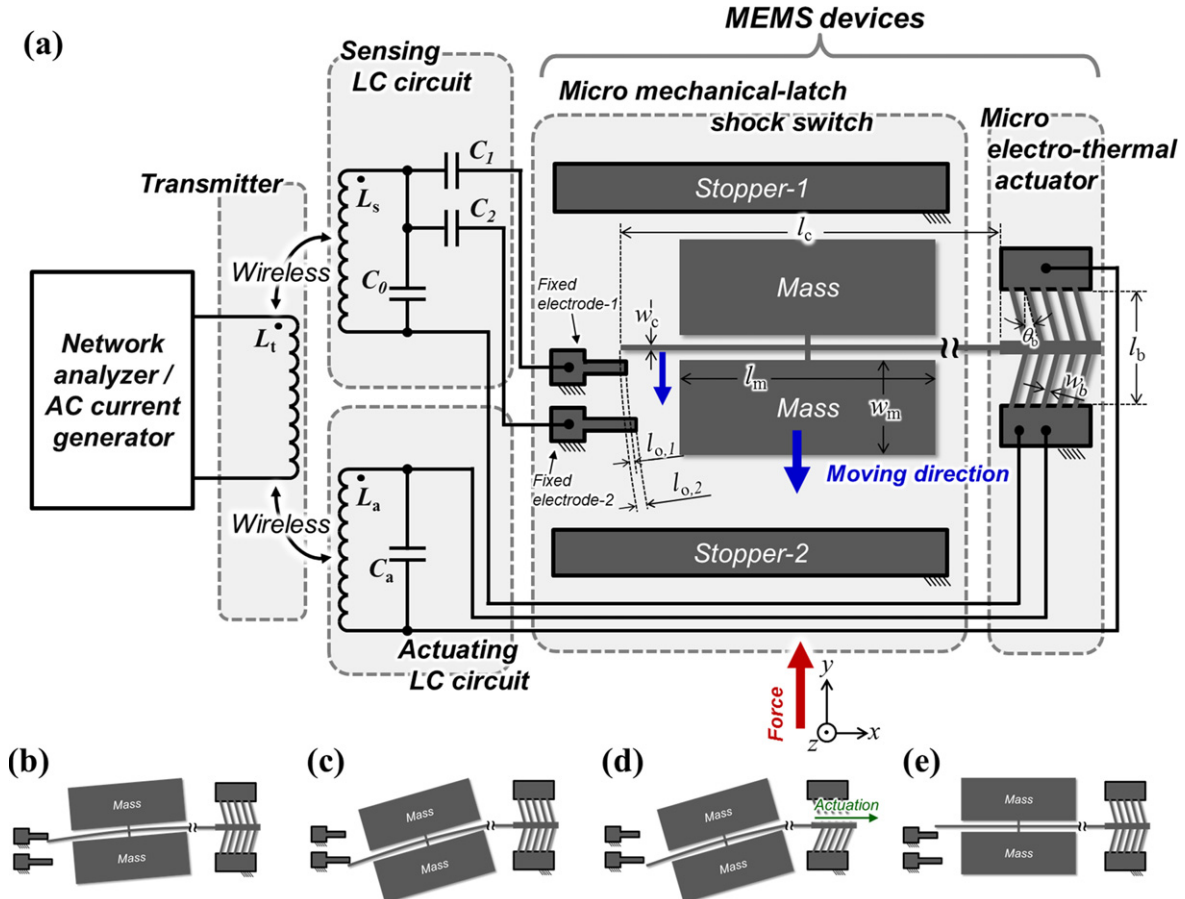


**Figure 2.** Illustrations of: (a) wirelessly readable and resettable shock recorder through the integration of LC circuits and MEMS devices in the original latching state; (b) in the 1st latching state of the micro mechanical-latch shock switch; (c) in the 2nd latching state; (d) during wireless actuation; (e) and back to the original state after the wireless actuation.

monitoring, then the switch needs to be resettable to function again.

Here, a reusable passive shock recorder is proposed by integrating LC circuits, a shock switch and a micro actuator. When the micro mechanical-latch shock switch connects to a sensing LC circuit experiences threshold acceleration, the latching state and the corresponding LC resonant frequency are changed. By connecting a micro actuator to an LC circuit, energy can be wirelessly sent to the micro actuator to reset the shock switch. In other words, the shock switch and the micro actuator do not need to be physically connected with any battery or power source. The shock event reading and resetting can be performed wirelessly through LC circuits. To the best of our knowledge, this is the first reusable passive shock recorder that combines both wireless sensing and wireless actuating functions through LC circuits.

## 2. Concept design

To record a shock event with a device with wireless reading and wireless resetting capabilities, a novel design, which integrates LC circuits and MEMS devices and includes a micro mechanical-latch shock switch and a micro electro-thermal actuator, is proposed, as shown in figure 2(a). The micro mechanical-latch shock switch is formed by a suspended beam, a suspended proof mass and fixed electrodes. While experiencing an external force in the  $+y$  direction, the suspended beam will deform and even touch the fixed electrode due to the inertia of the proof mass. When the external force reaches the threshold level, which is related to the overlapping length  $l_o$ , the free end of the suspended beam will flip over and latch to the fixed electrode. Then, the experienced shock level is recorded by the latching state, as shown in figures 2(b) and (c). When there are multiple fixed electrodes that form different overlapping lengths, different levels of shock can be recorded. Here, two different overlapping lengths ( $l_{o,1}$  and  $l_{o,2}$ ) and three latching states (original, 1st and 2nd latching states) are designed. Since the fixed electrodes and the anchor of the beam are wired to the sensing LC circuit, the micro mechanical-latch shock switch, which is formed by conductive material, is also an electrical switch in the sensing LC circuit. When different capacitors,  $C_0$ ,  $C_1$ ,  $C_2$ , are connected to the anchor and to fixed electrode-1 and to fixed electrode-2, respectively, the resonant frequency of the sensing LC circuit can be affected by the electrical switch. For example, if the device experiences a sufficient external force and switches from the original state to the 1st latching state, the equivalent capacitance changes from  $C_0$  to  $C_0 + C_1$ . Then, the resonant frequency shifts from  $(2\pi(L_s C_0)^{0.5})^{-1}$  to  $(2\pi(L_s(C_0 + C_1)^{0.5})^{-1}$ . Therefore, the latching state can be obtained wirelessly by monitoring the resonant frequency through a network analyzer connected with a transmitter. That is, the recorded shock level can be read wirelessly. Fixed stopper-1 and stopper-2 are designed to limit the maximum displacement of the proof mass. To reset the latching state, a micro electro-thermal bent-beam actuator [31] is designed at the other end of beam. With an actuating LC circuit

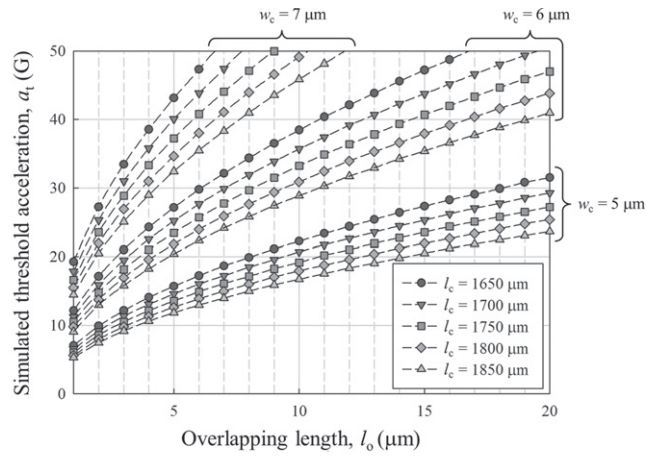


**Figure 3.** Simulated threshold accelerations of the mechanical-latch shock switch at various overlapping lengths with different beam lengths  $l_c$  and widths  $w_c$ .

electrically connected to the micro actuator, the wireless actuation can be performed to pull the beam horizontally. Therefore, when the actuating displacement is larger than the overlapping length, the latching state can be reset, as shown in figures 2(d) and (e), which means that the shock recorder can be reused.

## 3. Detailed design

### 3.1. Mechanical-latch shock switch

To design the micro mechanical-latch shock switch with the desired threshold accelerations, simulations were performed to decide the detailed dimensions. The beam length and width are denoted by  $l_c$  and  $w_c$ , respectively, as shown in figure 2(a). The proof mass length is  $l_m = 1500 \mu\text{m}$ , and the width is  $w_m = 620 \mu\text{m}$  made by nickel (Ni, Young's modulus 154.0 GPa, density 8880 kg m<sup>-3</sup>) [32]; the threshold accelerations of a mechanical-latch shock switch with different overlapping lengths  $l_o$ , beam lengths  $l_c$  and beam widths  $w_c$  are simulated by an analytical model with a fixed-roller boundary condition [33]. The thicknesses of the beam and proof mass are designed to be the same, 20  $\mu\text{m}$ , since they are designed to be fabricated through electroplating at the same time. Simulated results are shown in figure 3. It is found that a larger overlapping length  $l_o$ , as well as a stiffer spring with a shorter beam length  $l_c$  or a wider beam width  $w_c$ , will lead to a larger threshold acceleration. To reduce the variation on the threshold acceleration due to dimensional inaccuracy from fabrication, a longer and narrower beam is more effective, as shown in figure 3. However, it may also lead to a suspended beam with low stiffness, which can cause stiction in fabrication. Therefore, the beam with length  $l_c = 1750 \mu\text{m}$  and width  $w_c = 6 \mu\text{m}$  is selected for the following simulations and experiments. To record the shock event in tens of Gs, two overlapping lengths,  $l_{o,1}$  and  $l_{o,2}$ , are designed to be 6.0  $\mu\text{m}$

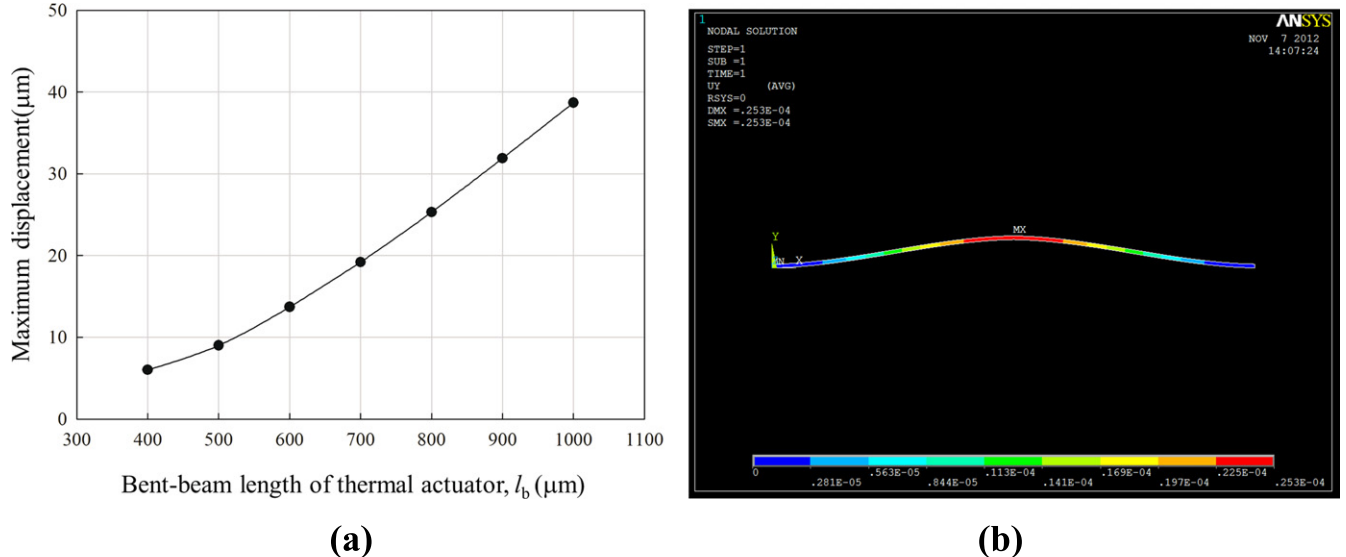


**Figure 4.** Simulated results: (a) maximum displacements of the micro electro-thermal bent-beam actuator with different bent-beam length  $l_b$ ; (b) simulated deformation of the micro electro-thermal bent-beam actuator with a bent-beam length of  $l_b = 800 \mu\text{m}$ .

and  $11.0 \mu\text{m}$  and to have threshold accelerations of  $25 \text{ G}$  and  $35 \text{ G}$ , respectively.

### 3.2. Electro-thermal bent-beam actuator

The maximum displacement of the electro-thermal actuator needs to be larger than the overlapping lengths to successfully reset the switch. To design the detailed dimensions of the micro actuator, a simulation is performed by the finite element method through the software ANSYS. In simulations, the highest temperature of the actuator is limited to  $400^\circ\text{C}$  to avoid degeneration of Ni [34]. The performances of the micro actuators with a different bent-beam length  $l_b$  are simulated with the bent angle  $\theta_b = 1^\circ$ , the bent-beam width  $w_b = 10 \mu\text{m}$ ,  $20 \mu\text{m}$  thickness, the coefficient of thermal expansion  $12.7 \times 10^{-6} \text{ K}^{-1}$ , Poisson's ratio 0.31, thermal conductivity  $90.5 \text{ W m}^{-1} \text{ K}^{-1}$ , specific heat  $443 \text{ J Kg}^{-1} \text{ K}^{-1}$  and resistivity  $13.5 \times 10^{-8} \Omega \text{ m}$ . Figure 4(a) shows the simulated maximum displacements at different bent-beam lengths, which happen at the apex of the bent-beam. Figure 4(b) shows one example simulated by ANSYS for bent-beam length =  $800 \mu\text{m}$ . With a longer bent-beam length, a larger displacement can be achieved. To reset the latching state, the micro actuator needs to displace a greater length than the overlapping length of the second latch,  $l_{o,2} = 11.0 \mu\text{m}$ . Therefore, the micro actuator with the  $600 \mu\text{m}$  bent-beam length should be enough to reset the latching state. Here, the bent-beam with a length of  $800 \mu\text{m}$  is selected to further ensure sufficient displacement. On the other hand, the micro actuator also works as a root support of the beam. To provide sufficient stiffness and output force in the horizontal ( $x$ ) direction, 10 sets of bent-beams are designed to provide a high spring constant in the  $x$  direction ( $k_x = 676.13 \text{ N m}^{-1}$ ). When the mechanical-latch shock switch experiences an unexpected acceleration of up to  $200 \text{ G}$  in the  $+x$  direction, the displacement of the actuator in the horizontal

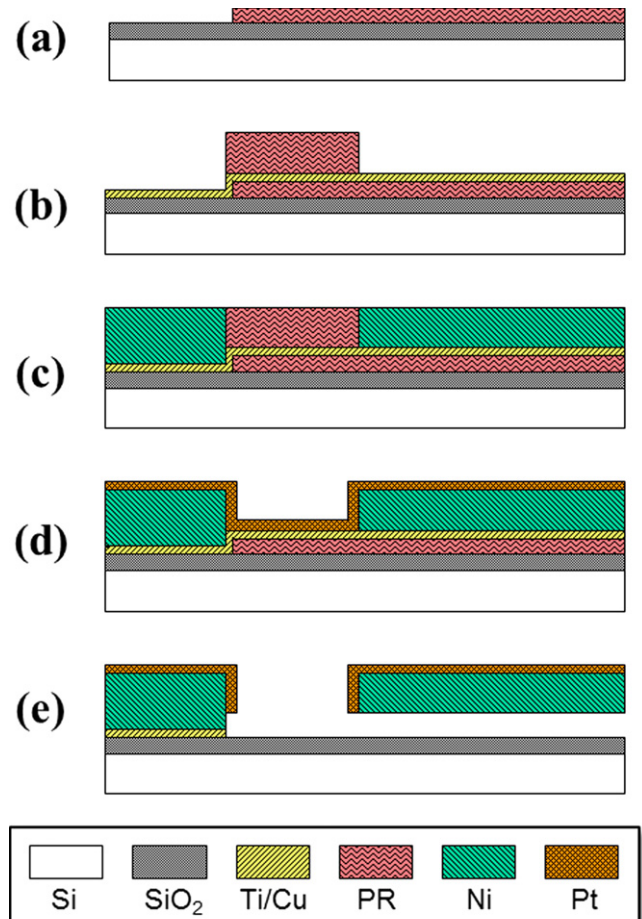


**Figure 5.** Fabrication process of the MEMS devices: (a) patterning the sacrificial layer (photoresist, PR) on the silicon wafer after oxidation; (b) sputtering the seed layer (Ti/Cu) and spin-coating the molding layer (PR); (c) electroplating the structure layer (Ni); (d) sputtering the conductive layer (Pt) and removing the molding layer; (e) removing the seed layer and the sacrificial layer to release the structure.

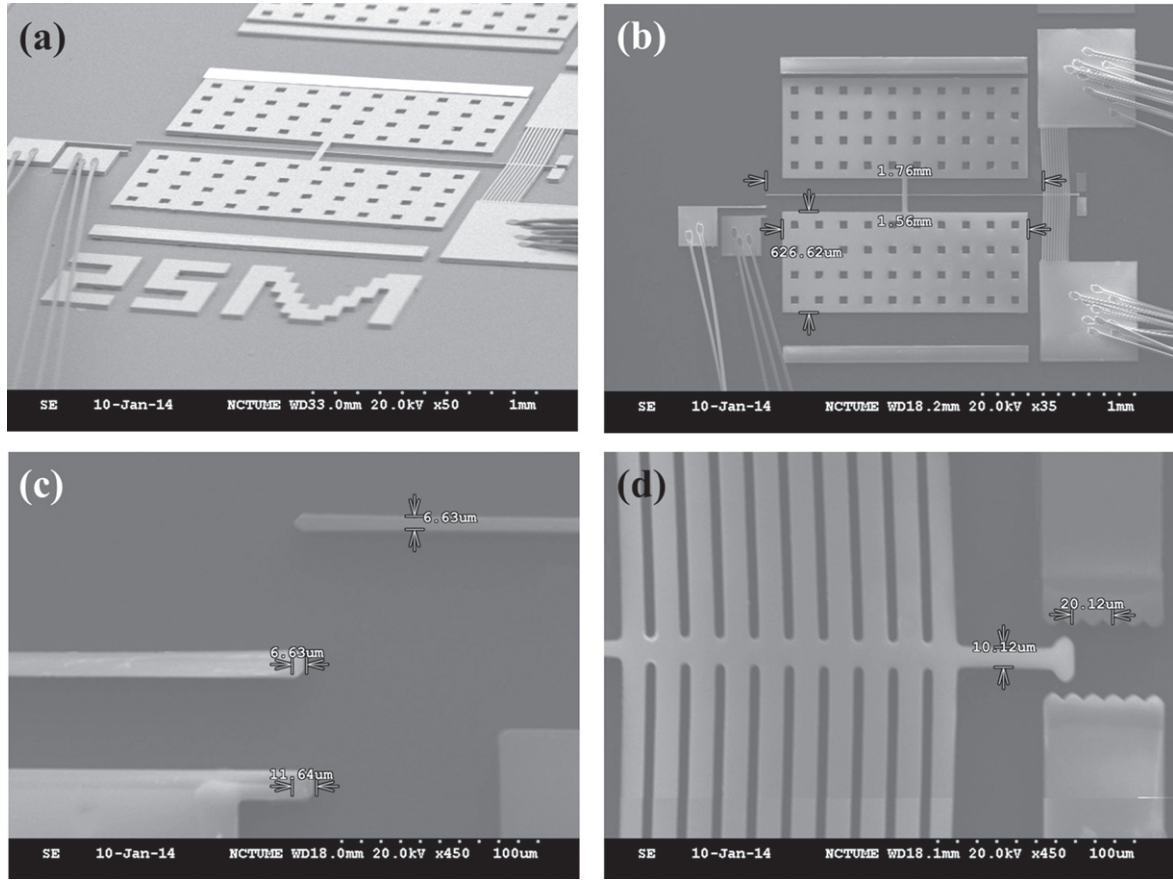


**Figure 6.** Photos of fabricated MEMS devices taken by scanning electron microscope Hitachi S-3000N: (a) bird's view; (b) top view; (c) closer view of the latching structure; (d) closer view of the bent-beam actuator.

direction is only  $0.88\ \mu\text{m}$ , which will not affect the latching state.

#### 4. Fabrication process and assembly

The fabrication process of the MEMS components is illustrated in figure 5. First, silicon dioxide thin film ( $1\ \mu\text{m}$ ) is grown on a silicon wafer as an electrical isolation layer through wet oxidation. Then, the photoresist FH-6400 (Fujifilm Olin) is coated and patterned to act as the sacrificial layer, as shown in figure 5(a). Then, 20 nm thick titanium (Ti) and 120 nm thick copper (Cu) are sputtered as the adhesion layer and as the seed layer for later electroplating, respectively. To form the structural layer, 27  $\mu\text{m}$  thick photoresist AZP-4620 is coated and patterned as the mold for Ni electroplating, as shown in figure 5(b). With the electroplating current density at  $0.8\ \text{mA cm}^{-2}$ , 20  $\mu\text{m}$  thick Ni is then electroplated to form the structure layer, as shown in figure 5(c). After removing the mold with acetone, 200 nm of platinum (Pt) thin film is further sputtered as the conductive layer for protection from oxidation, as shown in figure 5(d). After etching the sacrificial layer with acetone, part of the Pt and Ti/Cu thin film is removed through lift-off, and then the structural layer is

released, as shown in figure 5(e). After wire bonding to an 8-pin dual in-line package (DIP), which is performed by Chipin Electronics Co., Ltd [35], micro devices are successfully fabricated, as shown in figures 6(a) and (b), where the 1st and 2nd overlapping lengths are found to be  $6.63\ \mu\text{m}$  and  $11.64\ \mu\text{m}$ , respectively, as shown in figure 6(c).

To further integrate the fabricated MEMS devices with the sensing and actuating LC circuits, a low-cost prototype design for the assembly is proposed, as illustrated in figure 7(a). First, the DIP (MEMS devices are inside) is inserted into the corresponding socket on a printed circuit board (PCB), which has sensing and actuating capacitors welded on. A polymethylmethacrylate (PMMA) board is fixed to the PCB by plastic screws, and the receiving inductor for sensing is formed by winding enameled insulated wire (diameter 0.23 mm), followed by another receiving inductor for actuation. Since the actuating LC circuit needs to receive more power for the actuation of the micro actuator, the outer inductor, which has a larger diameter and better coupling, acts as the actuating inductor. After connecting the inductors and capacitors through welding, the device assembly is completed, as shown in figures 7(b) and (c). The length, width and height of the assembled device are 45 mm, 45 mm and 11 mm, respectively.

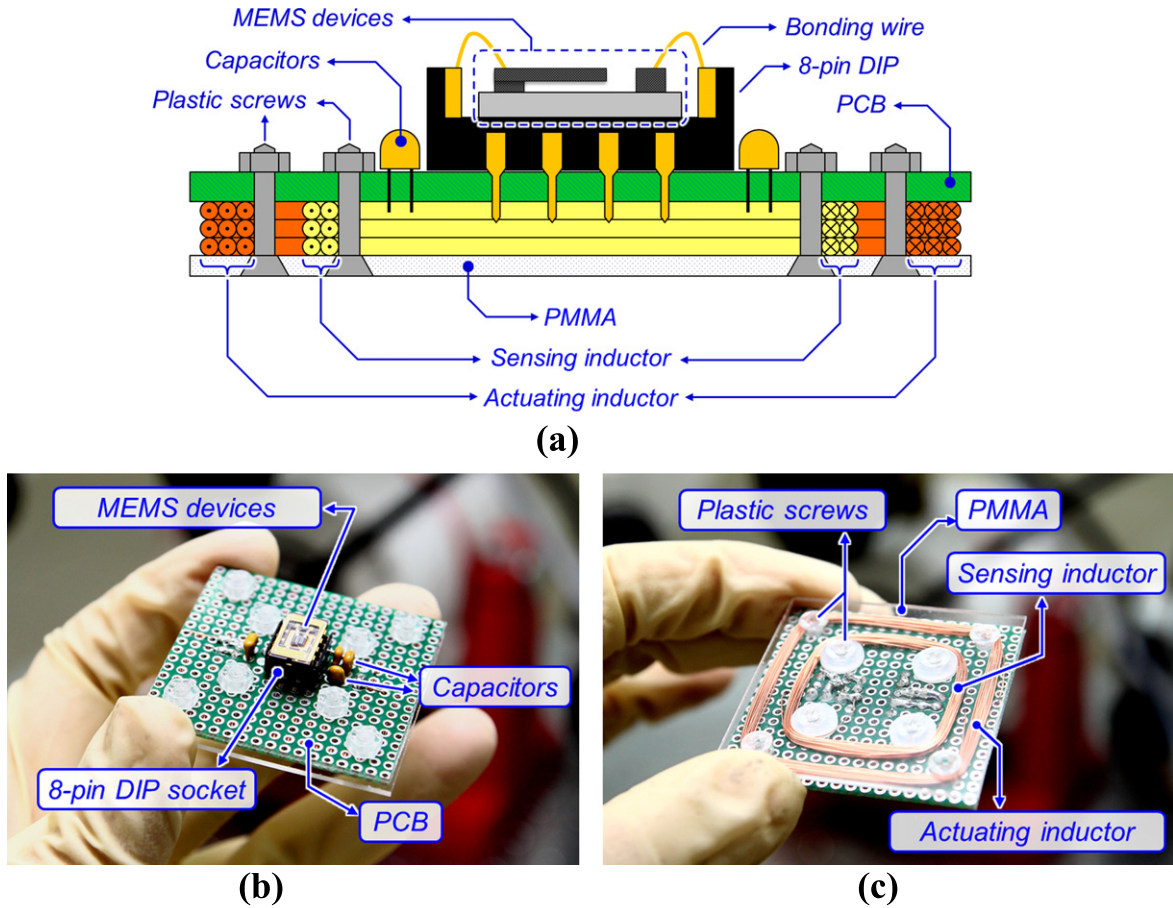


**Figure 7.** Assembly: (a) illustration of the assembly design; (b) the assembled device; (c) backside of the assembled device.

## 5. Test results and discussions

The shock recording, wireless reading and wireless actuating functions are first tested separately. Then, the integrated shock recorder is reset and tested again to verify the reusable function. The discrepancy between the simulation and the measurement results on the threshold acceleration and the sensing LC resonant frequency are also discussed.

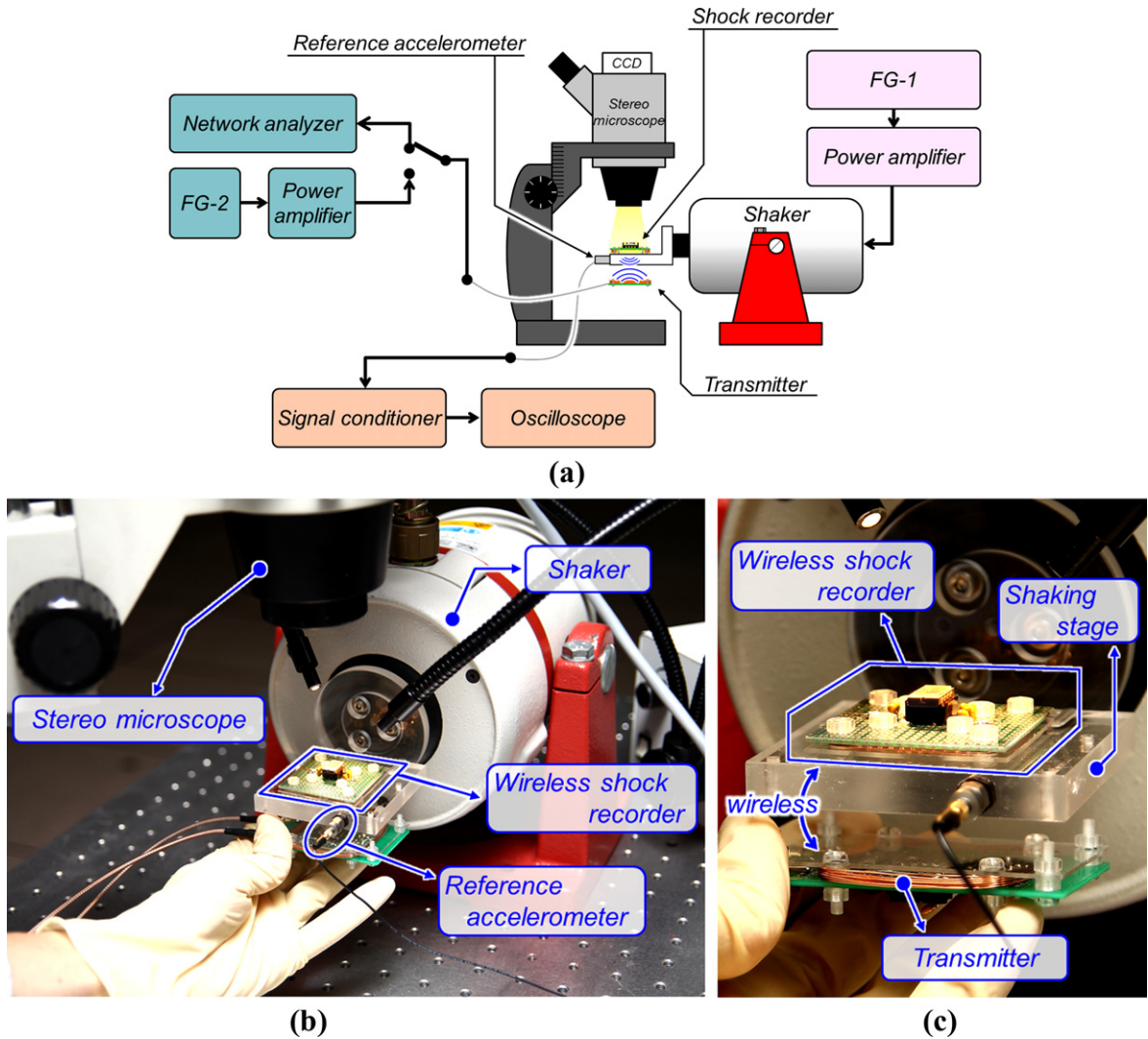
### 5.1. Testing setup

Figure 8 shows the overall testing setup of the proposed shock recorder. The assembled device is mounted on the stage of the shaker LDS V406. With a function generator (FG-1) Agilent 33210A controlling the signal waveform, the signal is amplified through power amplifier LDS PA100E and sent to the shaker to apply acceleration to the assembled device. The applied acceleration is monitored through the commercial accelerometer PCB Model 352C66 with signal conditioner PCB Model 480C02. The resonant frequency of the sensing LC circuit is wirelessly measured through the network analyzer HP 8751A that is connected with a transmitter (inductance  $17.11 \mu\text{H}$  and resistance  $0.31 \Omega$ ), which is made in the same manner as sensing/actuating inductors. With another function generator (FG-2) Agilent 33522A controlling the signal waveform, the in-house power amplifier can output a signal with a higher current. In the in-house power amplifier,

the signal from FG-2 is amplified by an operational amplifier (Texas Instruments OPA454) first and then sent to transistors (STMicroelectronics 2N3055 and MJ2955) to control the current output [36]. With dc supplier (King Instrument Electronics DPS-1603D) providing  $\pm 15 \text{ V}_{\text{DC}}$  to the operational amplifier and transistors, a  $2.25 \text{ A}_{\text{AC}} - 1.15 \text{ A}_{\text{AC}}$  current with a frequency of  $10 \text{ kHz} - 37 \text{ kHz}$  can be sent to the transmitter. Corresponding waveforms, impedances and currents are measured by Agilent oscilloscope DSO 1004A, impedance analyzer 4294A, and multimeter 34401A, respectively. The latching state of the micro mechanical-latch shock switch is monitored through a stereo microscope above the device.

### 5.2. Shock recording and wireless reading test

Figure 9 shows the shock recording test results. Before applying any acceleration, the mechanical-latch shock switch remains at the original latching state, as shown in figures 9(a) and (b). When the sensing inductance is  $L_s = 16.2 \mu\text{H}$ , and the capacitances are  $C_0 = 10.1 \text{ pF}$ ,  $C_1 = 5.0 \text{ pF}$  and  $C_2 = 15.3 \text{ pF}$ , the resonant frequency of the sensing LC circuit is found to be  $10.16 \text{ MHz}$ , as shown in figure 9(c), which is measured at the wireless distance of  $4 \text{ cm}$ . By gradually increasing the acceleration, when the acceleration reaches  $28.15 \text{ G}$ , the shock switch is found to change to the 1st latching state, as shown in figure 9(d). The resonant frequency of the sensing



**Figure 8.** Testing setup: (a) illustration of the testing system; (b) photo of the testing setup; (c) close view of the testing setup.

LC circuit is also found to shift to 9.18 MHz, as shown in figure 9(e). When the applied acceleration reaches

38.57 G, the shock switch changes to the 2nd latching state, as shown in figure 9(f). The resonant frequency of the sensing LC circuit is found to decrease to 7.84 MHz, as shown in figure 9(g). The applied accelerations and corresponding resonant frequencies of the sensing LC circuit are summarized in figure 10, which verify the capabilities of shock recording and wireless reading of the assembled device.

### 5.3. Wireless actuation test

To verify the wireless actuation function, a micro electro-thermal actuator without a mechanical-latch shock switch is first fabricated and tested. The inductance of the actuating inductor is calculated [37], and then the resonant frequency of the actuating LC circuits can be simulated by equation (1). Five different actuating LC circuits, which are connected to the micro actuator with different capacitances and resonant frequencies, are tested, as listed in table 1. By sending  $2.25 A_{AC} - 1.15 A_{AC}$  with a frequency of 10 kHz–37 kHz to

the transmitter, a wirelessly induced current in the micro actuator can be monitored by a serially connected multimeter. The measured results at the wireless distance of 4 cm are shown in figure 11. The corresponding resonant frequencies, in which the maximum currents are induced for LC-1 to LC-5, are found to be 14.0 kHz, 15.0 kHz, 17.0 kHz, 20.0 kHz and 31.0 kHz, respectively. In general, the LC circuit with the lower capacitance and higher resonant frequency should be able to receive and produce higher power at its resonant frequency due to a higher quality factor [38]; however, the current from the in-house power amplifier to the transmitter may also decrease with the increasing operating frequency. Here, the highest induced current is found to be LC-4 at  $f_{in} = 20$  kHz, as shown in figure 11. Since a high induced current is helpful in wireless actuation, LC-4 is chosen for the following wireless actuating tests. The actuations of the bent-beam actuator with LC-4 under different input frequencies  $f_{in}$  are tested and shown in figure 12. The largest displacement is at about  $13.6 \mu\text{m}$  at  $f_{in} = 20$  kHz, which is larger than the 2nd overlapping length of  $11.60 \mu\text{m}$ . To further enhance the power transmission from the transmitter to the actuating LC

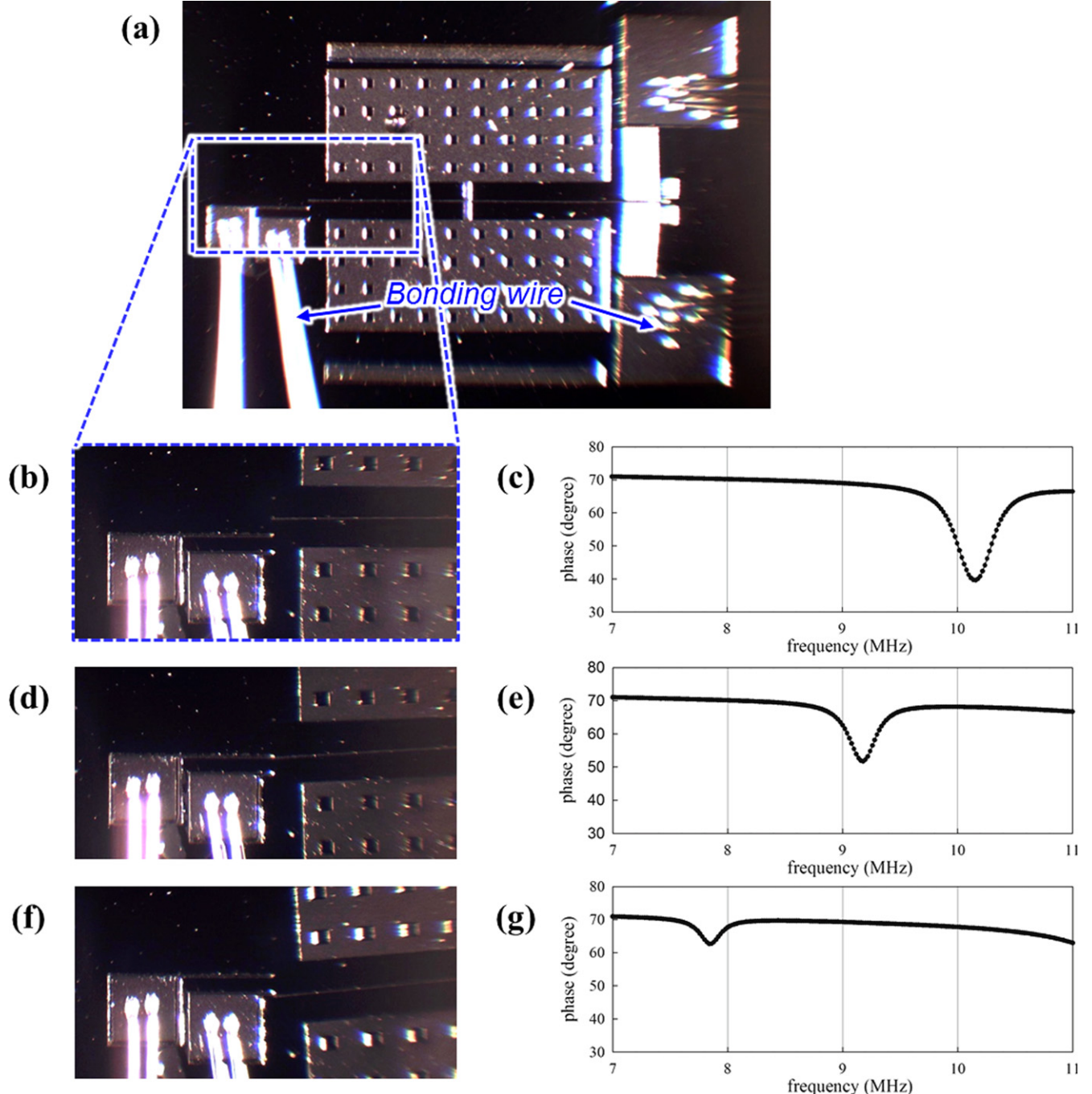


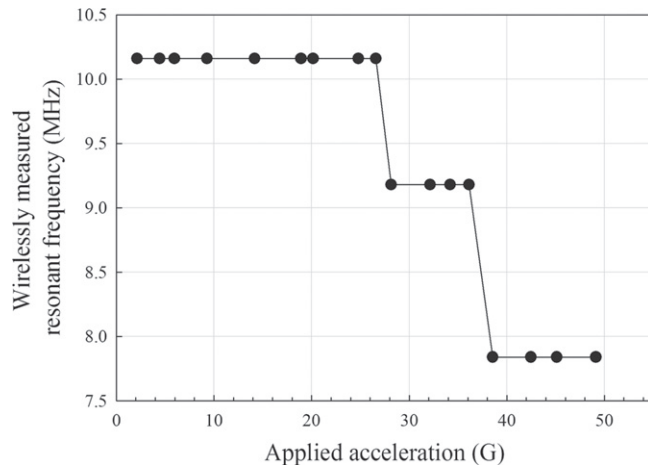
**Figure 9.** Shock recording and wireless reading test results: (a) top view of the MEMS devices before applying acceleration; (b) closer view of the latch structure; (c) wirelessly obtained frequency response of the device; (d) 1st latching state; (e) frequency response of the sensing LC circuit with the MEMS component at the 1st latching state; (f) at the 2nd latching state; (g) frequency response of the sensing LC circuit with the MEMS component at the 2nd latching state.

circuits, different compensation topologies [39] can be considered in the future.

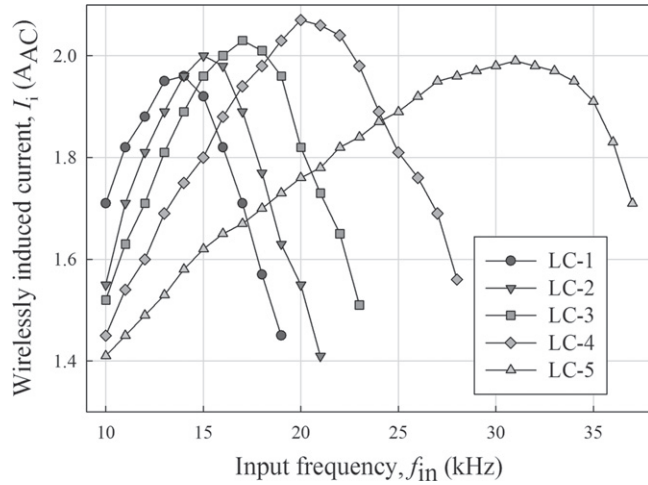
#### 5.4. Resetting and repeating shock tests

Based on the above test results on shock recording, wireless reading and wireless actuation, the integrated shock recorder was further tested to verify its wireless resetting and reusable capabilities. With the transmitting

current  $1.77 \text{ A}_{\text{AC}}$ , a current of  $2.07 \text{ A}_{\text{AC}}$  is induced at the actuating LC circuit to flow through the micro actuator at  $f_{\text{in}} = 20 \text{ kHz}$ . The micro shock switch can be successfully reset from the 2nd latching state back to the original latching state, as shown in figure 13. The shock tests after the reset are then performed for four additional cycles. The corresponding wirelessly measured resonant frequencies are summarized in figure 14, which shows, with considerable stability, the repeatable two-level shock recording



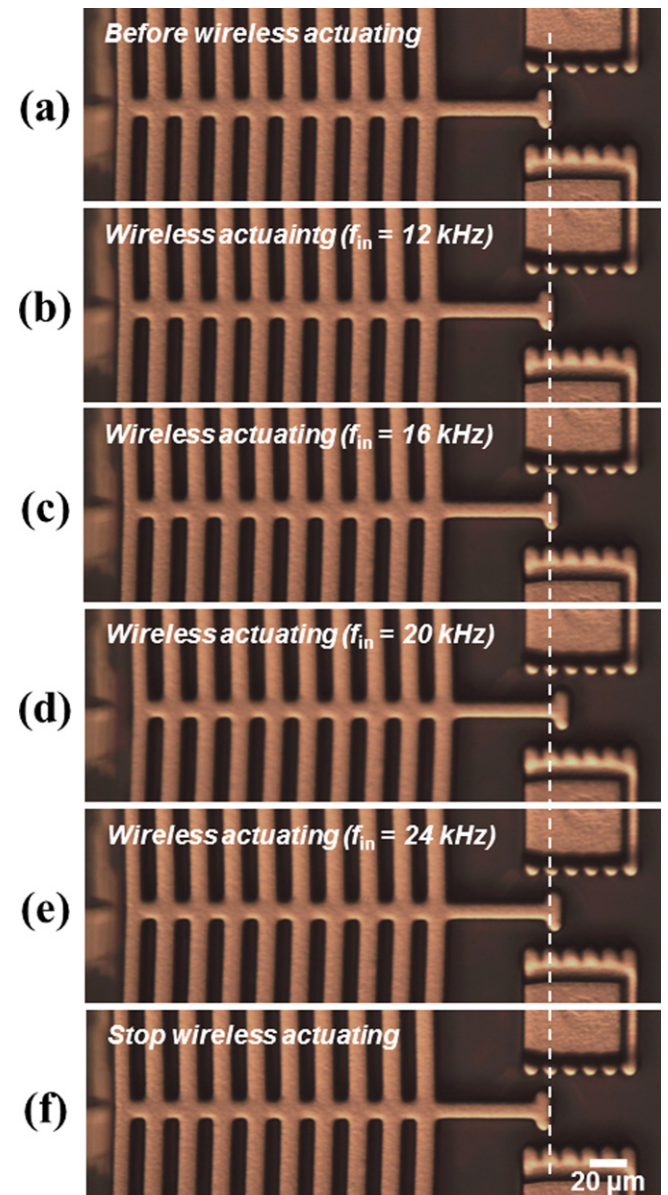
**Figure 10.** Applied accelerations and corresponding resonant frequencies of the sensing LC circuit.



**Figure 11.** Measured results of the wirelessly induced currents in a micro electro-thermal actuator with different actuating LC circuits.

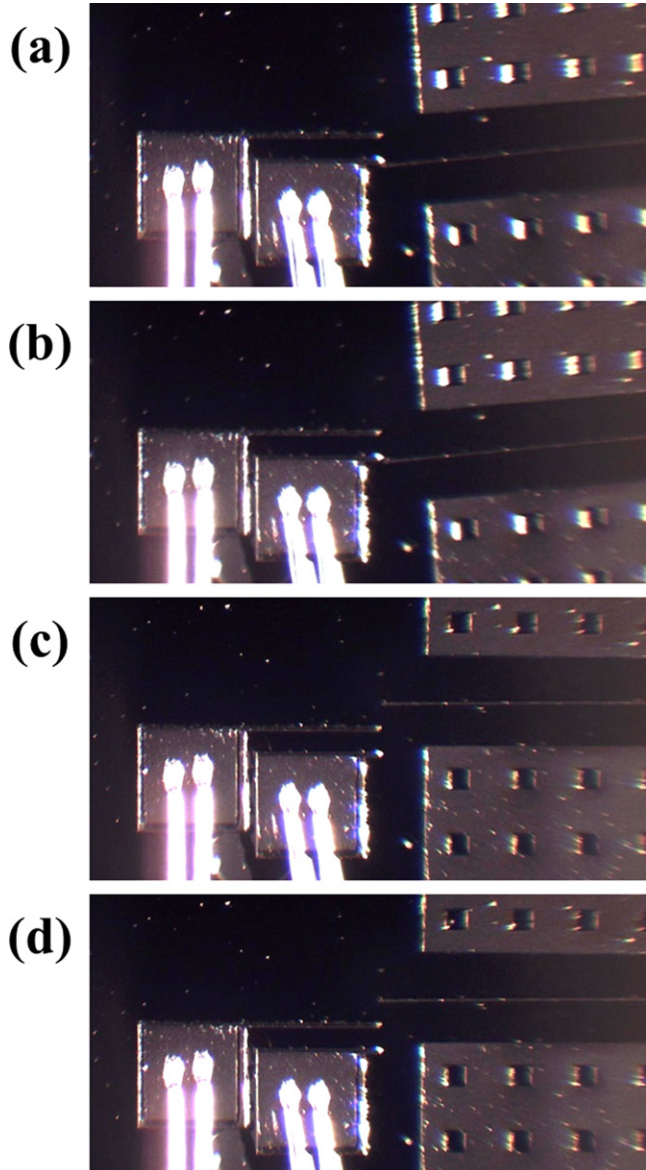
capabilities. The threshold acceleration to the first latching state remains in the range of 28.06 G to 29.18 G, and the threshold acceleration to the second latching state remains in the range of 37.10 G to 39.44 G. In the 6th & 7th shock and resetting tests, the micro mechanical-latch shock switch still works normally, but the resonant frequency of the sensing LC circuit doesn't shift with the change of latching state. Although the suspended beam contacts fixed electrodes under different latching states, the contact resistances between the suspended beam and the fixed electrodes after 5 cycles are found to change from the initial  $6\Omega$  to higher than  $100\text{ M}\Omega$ , which is the upper limit of multimeter 34401A. The wear of conductive layer Pt is believed to be the reason for the failure. An alternative conductive layer with a better anti-wear characteristic, such as TiC or TiN [40], can be utilized instead of Pt in the future to further enhance the life time.

Table 2 summarizes the simulation and the measurement results on the threshold accelerations and resonant frequencies at different latching states; the simulations are based on the



**Figure 12.** Wireless actuating test results of the micro electro-thermal actuator with actuating circuit LC-4: (a) before wireless actuating; (b) wireless actuating with input frequency  $f_{\text{in}} = 12\text{ kHz}$ ; (c) input frequency  $f_{\text{in}} = 16\text{ kHz}$ ; (d) input frequency  $f_{\text{in}} = 20\text{ kHz}$ ; (e) input frequency  $f_{\text{in}} = 24\text{ kHz}$ ; (f) stop wireless actuating.

measured dimensions from the SEM photos of the fabricated devices. The measured threshold accelerations are the result of 5 continuous shock recording-reset tests. The deviations of the measured threshold accelerations at 1st and 2nd latching states between the five tests are less than 1.2 G and 2.4 G, respectively. The measured resonant frequencies in table 2 are the average of 5 shock recording-reset tests. The errors between the simulated and measured resonant frequency at the original unlatched state are larger, which could be caused by the closely wounded inductor with a large stray capacitance [41]. However, the discrepancy between the simulated and measured average resonant frequency becomes smaller at the 1st and 2nd latching states.



**Figure 13.** Closer view of the latching structure: (a) 2nd latching state before wireless actuating; (b) wireless actuating with input frequency  $f_{in} = 16$  kHz; (c) wireless actuating with input frequency  $f_{in} = 20$  kHz; (d) stop wireless actuating.

**Table 1.** Detailed parameters of the actuating LC circuits.

	$C_a$ , selected ( $\mu\text{F}$ )	$L_a$ , simulated ( $\mu\text{H}$ )	$f_a$ , simulated (kHz)
LC-1	11.13	14.32	12.68
LC-2	8.84	14.32	14.18
LC-3	6.63	14.32	16.37
LC-4	4.42	14.32	20.05
LC-5	2.21	14.32	28.36

## 6. Conclusions

Here, a reusable passive shock recorder is designed, fabricated and tested to record a shock event for tens of Gs with

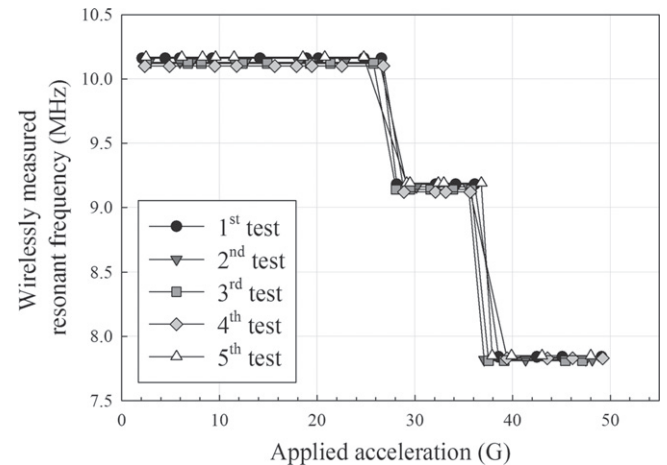


**Figure 14.** Applied accelerations and corresponding measured resonant frequencies in five repeating shock recording-reset tests.

**Table 2.** Simulation and measurement results of the threshold acceleration and the sensing LC resonant frequency.

	Threshold acceleration (G)		Sensing LC resonant frequency, $f$ (MHz)	
	Simulated	Measured	Simulated	Measured
Original state	—	—	12.72	10.14
1st latching state	26.66	28.06–29.18	10.39	9.16
2nd latching state	35.27	37.10–39.44	8.05	7.83

wireless reading and wireless resetting capabilities through the integration of LC circuits and MEMS devices. When the micro mechanical-latch shock switch connected to the sensing LC circuit experiences threshold accelerations, the latching state and the corresponding LC resonant frequency are changed. When a micro electro-thermal actuator is connected to the actuating LC circuit, the energy can be wirelessly sent to the micro actuator to unlatch the shock switch. The shock switch and micro actuator do not need to be physically connected with any battery or power source. The shock event reading and resetting can be performed wirelessly through LC circuits. Therefore, the shock recorder can be used repeatedly. The fabricated shock recorder is repeatedly tested for five cycles and shown to function successfully. To the best of our knowledge, this is the first passive shock recorder that combines both wireless sensing and wireless resetting capabilities, which makes it reusable and suitable to place in an environment where the battery is hard to replace.

## Acknowledgments

This work was supported by the National Science Council of Taiwan under Grant NSC 102-2625-M-009-005. The authors would also like to acknowledge Prof Jin-Chern Chiou, Prof

Tsung-Lin Chen, and Prof Ching-Chung Yin for providing the measurement facilities.

## References

- [1] Leung A M, Ko W H, Spear T M and Bettice J A 1986 Intracranial pressure telemetry system using semicustom integrated circuits *IEEE Trans. Biomed. Eng.* **33** 386–95
- [2] Todoroki A, Miyatani S and Shimamura Y 2003 Wireless strain monitoring using electrical capacitance change of tire: part I—with oscillating circuit *Smart Mater. Struct.* **12** 403–9
- [3] Huang P-L, Kuo P-H, Huang Y-J, Liao H-H, Yang Y-J J, Wang T, Wang Y-H and Lu S-S 2012 A controlled-release drug delivery system on a chip using electrolysis *IEEE Trans. Ind. Electron.* **59** 1578–87
- [4] Ong K G, Grimes C A, Robbins C L and Singh R S 2001 Design and application of a wireless, passive, resonant-circuit environmental monitoring sensor *Sensors Actuators A* **93** 33–43
- [5] Shin K H, Moon C R, Lee T H, Lim C H and Kim Y J 2005 Flexible wireless pressure sensor module *Sensors Actuators A* **123/124** 30–5
- [6] Ong K G and Grimes C A 2000 A resonant printed-circuit sensor for remote query monitoring of environmental parameters *Smart Mater. Struct.* **9** 421–8
- [7] Rosengren L, Bäcklund Y, Sjöström T, Hök B and Svedbergh B 1992 A system for wireless intra-ocular pressure measurements using a silicon micromachined sensor *J. Micromech. Microeng.* **2** 202–4
- [8] Akar O, Akin T and Najafi K 2001 A wireless batch sealed absolute capacitive pressure sensor *Sensors Actuators A* **95** 29–38
- [9] Fonseca M A, English J M, Arx M V and Allen M G 2002 Wireless micromachined ceramic pressure sensor for high-temperature applications *J. Microelectromech. Syst.* **11** 337–43
- [10] Chen P-J, Rodger D C, Saati S, Humayun M S and Tai Y-C 2008 Microfabricated implantable parylene-based wireless passive intraocular pressure sensors *J. Microelectromech. Syst.* **17** 1342–51
- [11] Baldi A, Choi W and Ziaie B 2003 A self-resonance frequency-modulated micromachined passive pressure transensor *IEEE Sensors J.* **3** 728–33
- [12] Jia Y, Sun K, Agosto F J and Quiñones M T 2006 Design and characterization of a passive wireless strain sensor *Meas. Sci. and Technol.* **17** 2869–76
- [13] Matsuzaki R and Todoroki A 2005 Passive wireless strain monitoring of tyres using capacitance and tuning frequency changes *Smart Mater. Struct.* **14** 561–8
- [14] Ludwig A, Frommberger M, Tewes M and Quandt E 2003 High-frequency magnetoelastic multilayer thin films and applications *IEEE Trans. Magn.* **39** 3062–7
- [15] Butler J C, Vigliotti A J, Verdi F W and Walsh S M 2002 Wireless, passive, resonant-circuit, inductively coupled, inductive strain sensor *Sensors Actuators A* **102** 61–6
- [16] Wu S Y and Hsu W 2013 Design and characterization of LC strain sensors with novel inductor for sensitivity enhancement *Smart Mater. Struct.* **22** 105015
- [17] DeHennis A D and Wise K D 2005 A wireless microsystem for the remote sensing of pressure, temperature, and relative humidity *J. Microelectromech. Syst.* **14** 12–22
- [18] Harpster T J, Hauvespre S, Dokmeci M R and Najafi K 2002 A passive humidity monitoring system for *in-situ* remote wireless testing of micropackages *J. Microelectromech. Syst.* **11** 61–7
- [19] Ong J B, You Z, Mills-Beale J, Tan E L, Pereles B D and Ong K G 2008 A wireless, passive embedded sensor for real-time monitoring of water content in civil engineering materials *IEEE Sensors J.* **8** 2053–8
- [20] Marioli D, Sardini E and Serpelloni M 2010 Passive hybrid MEMS for high-temperature telemetric measurements *IEEE Trans. Instrum. Meas.* **59** 1353–61
- [21] García-Cantón J, Merlos A and Baldi A 2007 A wireless LC chemical sensor based on a high quality factor EIS capacitor *Sensors Actuators B* **126** 648–54
- [22] Sridhar V and Takahata K 2008 A hydrogel-based wireless sensor using micromachined variable inductors with folded flex-circuit structures for biomedical applications *Proc. IEEE Int. Conf. on Micro Electro. Mechanical Systems 2008 (Tucson, AZ, Jan 13–17)* pp 70–3
- [23] Ong K G, Bitler J S, Grimes C A, Puckett L G and Bachas L G 2002 Remote query resonant-circuit sensors for monitoring of bacteria growth: application to food quality control *Sensors* **2** 219–32
- [24] Ong K G, Zeng K and Grimes C A 2002 A wireless, passive carbon nanotube-based gas sensor *IEEE Sensors J.* **2** 82–8
- [25] Mita Y et al 2009 Demonstration of a wireless driven MEMS pond skater that uses EWOD technology *Solid-State Electron.* **53** 798–802
- [26] Ryu K, Zueger J, Chung S K and Cho S K 2010 Underwater propulsion using ac-electrowetting-actuated oscillating bubbles for swimming robots *Proc. IEEE Int. Conf. on Micro Electro. Mechanical Systems 2010 (Wanchai, Hong Kong, Jan 24–28)* pp 160–3
- [27] Rahimi S, Sarraf E H, Wong K and Takahata K 2011 Implantable drug delivery device using frequency-controlled wireless hydrogel microvalves *Biomed. Microdevices* **13** 267–77
- [28] Ali M S M and Takahata K 2011 Wireless microfluidic control with integrated shape-memory-alloy actuators operated by field frequency modulation *J. Micromech. Microeng.* **21** 075005
- [29] Li P Y, Sheybani R, Kuo J T W and Meng E 2009 A parylene bellows electrochemical actuator for intraocular drug delivery *Transducers'09: 15th Int. Conf. Solid-State Sensors, Actuators and Microsystems (Denver, CO, June 21–25)* pp 1461–4
- [30] Kuo J-C, Kuo P-H, Lai Y-T, Ma C-W, Lu S-S and Yang Y-J J 2013 A passive inertial switch using MWCNT–hydrogel composite with wireless interrogation capability *J. Microelectromech. Syst.* **22** 646–54
- [31] Sinclair M J 2000 A high force low area MEMS thermal actuator *Proc. 7th Intersociety Conf. on Thermal Phenomena* vol 1 (Las Vegas, NV) pp 127–32
- [32] Lee C-Y, Li M-H, Cheng Y-T, Hsu W and Li S-S 2012 Electroplated Ni-CNT nanocomposite for micromechanical resonator applications *IEEE Electron Device Lett.* **33** 872–4
- [33] Chung C H, Ma R-P, Shieh Y-C and Hsu W 2011 A robust micro mechanical-latch shock switch with low contact resistance *Transducers'11: 16th Int. Conf. Solid-State Sensors, Actuators and Microsystems (Beijing, China, June 5–9)* pp 1046–51
- [34] Que L, Park J-S and Gianchandani Y B 2001 Bent-beam electrothermal actuators—part I: single beam and cascaded devices *J. Microelectromech. Syst.* **10** 247–54
- [35] Chipin Electronics Company Limited (Zhubei City, Hsinchu County, Taiwan) <http://yp.518.com.tw/ypweb-index-198747.html>
- [36] Texas Instruments (Dallas, Texas, USA) operational amplifier OPA454 datasheet <http://www.ti.com/lit/ds/symlink/opa454.pdf>
- [37] Wheeler H A 1928 Simple inductance formulas for radio coils *Proc. of the Institute of Radio Engineers* **16** 1398–400

[38] RamRakhani A K, Mirabbasi S and Chiao M 2011 Design and optimization of resonance-based efficient wireless power delivery systems for biomedical implants *IEEE Trans. Biomed. Circuits Syst.* **5** 48–63

[39] Stielau O H and Covic G A 2000 Design of loosely coupled inductive power transfer systems *Int. Conf. on Power System Technology 2000* vol 1 (*Perth, Australia, Dec. 4-7*) pp 85–90

[40] Walkowicz J, Smolik J, Miernik K and Bujak J 1996 Anti-wear properties of Ti(C, N) layers deposited by the vacuum arc method *Surf. Coat. Technol.* **81** 201–8

[41] Grandi G, Kazimierczuk M K, Massarini A and Reggiani U 1999 Stray capacitances of single-layer solenoid air-core inductors *IEEE Trans. Ind. Appl.* **35** 1162–8